International Journal of Mechanical, Industrial and Aerospace Sciences
ISSN: 2517-9950
Vol:5, No:1, 2011

Assessment of the Accuracy of Spalart-Allmaras Turbulence Model for Application in Turbulent Wall Jets

A. M. Tahsini

***Abstract*—**The Spalart and Allmaras turbulence model has been implemented in a numerical code to study the compressible turbulent flows, which the system of governing equations is solved with a finite volume approach using a structured grid. The AUSM$^+$ scheme is used to calculate the inviscid fluxes. Different benchmark problems have been computed to validate the implementation and numerical results are shown. A special Attention is paid to wall jet applications. In this study, the jet is submitted to various wall boundary conditions (adiabatic or uniform heat flux) in forced convection regime and both two-dimensional and axisymmetric wall jets are considered. The comparison between the numerical results and experimental data has given the validity of this turbulence model to study the turbulent wall jets especially in engineering applications.

***Keywords*—**Wall Jet, Heat transfer, Numerical Simulation, Spalart-Allmaras Turbulence model.

I. Introduction

TURBULENT wall jets are widely used in many engineering processes such as inlet devices in ventilation, separation control in airfoils and film cooling of turbine blades. The fluid is injected at high velocity tangentially to a plane plate. The resulting flow can be viewed as a combination of an inner wall boundary layer, where the velocity increases from zero at the wall to a local maximum and an outer free jet where the velocity decreases from a local maximum to zero or to the free stream value in the case of moving surrounding. The interaction between the large turbulence scales of the external layer and the smaller scales of the internal layer is at the origin of the complexity of the flow. Thus, this type of flow has been the subject of several experimental studies that have been devoted to either the kinematics or the thermal aspects of the problem. [1]-[4]

The review of the numerical works, conducted about turbulent wall jets shows that this type of flow has been studied with different turbulence models. Kechiche et al. [5] have used a low Reynolds number k-ε model with different damping functions, in order to explore the behaviour of two dimensional turbulent wall jets. Craft et al. [6] have described the application of different levels of turbulence closure and near wall treatment to the computation of 2D downward directed wall jet that encounters an upward moving flow. Kechiche et al. [7] have also studied the influence of the inlet conditions at the nozzle exit on the jet characteristic parameters. Cho and Park [8] have discussed a computational procedures and results of an upwash jet arising from two opposing plane wall jets.

The Spalart and Allmaras (S-A) turbulence model has not been validated to use in turbulent wall jets with heat transfer. The S-A model is not derived from the k–ε equations and it is deeply empirical. This is a one-equation model that solves a transport equation for turbulent eddy viscosity itself, instead of specifying it with a characteristic velocity and length scales. It has been specifically developed for wall-bounded aerodynamic flows with adverse pressure gradients. This model is a low Reynolds number model, which can be directly applied throughout the boundary layer if the near wall mesh is fine enough to resolve the gradients. It has been implemented by many groups providing good results in a wide range of different applications [9]-[12]. Nevertheless the behaviour of this turbulence model in the wall jet flows modelling is little known. The purpose of the present study is to review its performance in this problem. Ability of this one-equation model to simulate the mentioned flows will be useful from the time cost of numerical simulation viewpoint, in comparison with the other complicated models.

II. Equations and Numerical Method

The equations governing the continuum flow of an ideal gas representing the conservation of mass, momentum, and energy are averaged using the Reynolds decomposition, results in Reynolds Averaged Navier-Stokes equations (RANS). These equations have the same general form as the instantaneous Navier-Stokes equations except the new term called 'Reynolds stress tensor'. This term represents the effect of smaller scales on the mean flow. It acts as an additional stress and dominates the transport processes several orders of magnitudes over the molecular transport. The conservation equations are written in the following integral form [13]:

$$\frac{\partial Q}{\partial t}+\frac{\partial(R+T)}{\partial x}+\frac{\partial(S+H)}{\partial y}+J\left(\frac{S+S'+H+H'}{y}\right)=0 \qquad (1)$$

A. M. Tahsini is assistant professor of the Aerospace Research Institute, Tehran, Iran (e-mail: a_m_tahsini@ yahoo.com).

$$Q=\begin{bmatrix}\rho\\ \rho u\\ \rho v\\ \rho E\end{bmatrix}\ R=\begin{bmatrix}\rho u\\ \rho uu+p\\ \rho uv\\ \rho uH\end{bmatrix}$$
$$S=\begin{bmatrix}\rho v\\ \rho vu\\ \rho vv+p\\ \rho vH\end{bmatrix}\ S'=\begin{bmatrix}0\\ 0\\ -p\\ 0\end{bmatrix} \quad (2)$$
$$T=\begin{bmatrix}0\\ -\tau_{xx}\\ -\tau_{xy}\\ q_x-u\tau_{xx}-v\tau_{xy}\end{bmatrix}$$
$$H=\begin{bmatrix}0\\ -\tau_{yx}\\ -\tau_{yy}\\ q_y-u\tau_{yx}-v\tau_{yy}\end{bmatrix}\ H'=\begin{bmatrix}0\\ 0\\ \tau_{\theta\theta}\\ 0\end{bmatrix}$$

$$\tau_{xx}=\mu_{eff}\left(2\frac{\partial u}{\partial x}-\frac{2}{3}\nabla.V\right)$$
$$\tau_{xy}=\mu_{eff}\left(\frac{\partial u}{\partial y}+\frac{\partial v}{\partial x}\right) \quad (3)$$
$$\tau_{yy}=\mu_{eff}\left(2\frac{\partial v}{\partial y}-\frac{2}{3}\nabla.V\right)$$
$$\tau_{\theta\theta}=\mu\left(2\frac{v}{y}-\frac{2}{3}\nabla.V\right)$$

$$E=C_vT+(uu+vv)/2$$
$$H=E+p/\rho \quad (4)$$
$$\mu_{eff}=\mu+\mu_t$$

Where ρ, u, v, E, p, H, μ, μ_t are density, axial velocity, lateral velocity, total internal energy, pressure, total enthalpy, molecular dynamic viscosity and turbulent dynamic viscosity, respectively. Parameter *J* is 0 in two dimensional and 1 in axisymmetric flow.

To close the RANS equations, individual Reynolds stress components can be solved throughout the flow field. The turbulence model retained to close the system of equations is S-A model [14]. This is a one equation model assembled using empiricism and arguments of dimensional analysis, Galilean invariance and selective dependence on the molecular viscosity. In this model, the eddy viscosity is computed through a partial differential equation. The defining equation for this model is written as follows. The first term on the right hand side of this equation is the production term. Moreover, the last term is the destruction term and the others are the diffusion terms. This equation is solved for the variable $\tilde{\nu}$ and the eddy viscosity is calculated as $\nu_t=\tilde{\nu}f_{v1}$ where the function f_{v1} is a damping function used to properly treat the buffer layer and the viscous sublayer. Here, d is the distance to the closest wall.

$$\frac{D(\tilde{\nu})}{Dt}=c_{b1}\tilde{S}\tilde{\nu}+\frac{1}{\sigma}\left[\nabla.((\nu+\tilde{\nu})\nabla\tilde{\nu})+c_{b2}(\nabla\tilde{\nu})^2\right]$$
$$-c_{w1}f_w\left(\frac{\tilde{\nu}}{d}\right)^2 \quad (5)$$

Where

$$\tilde{S}=S+\left(\tilde{\nu}/\kappa^2d^2\right)f_{v2}$$
$$f_{v2}=1-X/(1+Xf_{v1})$$
$$f_{v1}=X^3/\left(X^3+c_{v1}^3\right) \quad (6)$$
$$X=\tilde{\nu}/\nu$$

Here S is the magnitude of vorticity and $\tilde{S}$ is modified strain rate. The function f_w is given as

$$f_w=g\left(\frac{1+c_{w3}^{\ 6}}{g^6+c_{w3}^{\ 6}}\right)^{\frac{1}{6}} \quad (7)$$

Where

$$g=r+c_{w2}\left(r^6-r\right)$$
$$r=\frac{\tilde{\nu}}{\tilde{S}\kappa^2d^2} \quad (8)$$

The constants are: $C_{b1}=0.1355$, $C_{b2}=0.622$, $C_{v1}=7.1$, $\sigma=2/3$, $C_{w1}=3.239$, $C_{w2}=0.3$, $C_{w3}=2$, $\kappa=0.41$. Equation 5 is solved coupled with flow governing equations.

Using a cell centred based finite volume scheme, the discrete vector of conserved variables is defined as an average over the cell of the continuous properties. The discrete property vector is:

$$Q_i=\frac{1}{V_i}\int_{V_i}QdV \quad (9)$$

This definition can be used to rewrite the Eq. (1), resulting:

$$\frac{\partial(V_iQ_i)}{\partial t}+\int_{S_i}\left[(R+T)dy-(S+H)dx\right]=0 \quad (10)$$

The time integration is accomplished by a fully explicit time stepping scheme. Moreover, the purpose of the spatial discretization scheme is to numerically evaluate the surface integral in Eq. (10). This approximation of the integral is different for the inviscid and the viscous flux terms. In this work, while the viscous terms are always treated using a central scheme, the inviscid terms is treated using a Liou's AUSM$^+$ scheme (Advection Upstream Splitting Scheme) to express the numerical flux at the cell faces [15]. This scheme

has following features: Positivity preserving property, improvement in accuracy, simplicity, and easy generalization to other conservation laws. The AUSM$^+$ scheme gives the numerical flux in the following expression:

$$F_{nL} = M_l \frac{a_l}{2}(\Phi_L + \Phi_R) - |M_l| \frac{a_l}{2} \Delta\Phi + \mathrm{P}_{nl} \qquad (11)$$

Noting that the flux terms account for only normal components of the flux at the face, $F_{nl} = \vec{F}_l . \vec{n}_l$ where $\vec{n}_l$ is the unit normal vector of the cell face. Details can be found in reference 13.

Appropriate boundary conditions are applied using ghost cells around the main field. Adjacent cells are used to find properties gradient on cell faces, required for evaluation of viscous terms. Gradients are computed here in the standard finite volume fashion, in which the derivatives are calculated in each volume considering that the discrete derivative in a given volume is the average on the volume of the derivative and, then, using Green's theorem to transform the computation of the derivative on the computation of the line integral. We have used the quadrilateral mesh for discretization. In the CFD simulations, the mesh should be fine enough to capture the flow gradients and reduce the numerical errors. In general, this is achieved by meshing by different number of grid elements and observes the change in a certain quantity of interest (grid independence study). This study has been done in all numerical simulations presented here. Grids are also refined enough to resolve the near wall gradients and laminar sublayer.

III. RESULTS AND DISCUSSION

To validate the behaviour of the laminar features of numerical procedure, different benchmark problems such as wind driven cavity, laminar flat plate and Poiseuille flow has been studied. The results have certified the accuracy of our numerical procedure. To assure the validity of described code, we here present results for two basic turbulent flows: First, computations are performed for a flow over a flat plate; then the case of backward facing step flow is considered.

Computing the turbulent flow over a flat plate is a good, initial validation study for turbulent flow solvers. Any good turbulence model should be able to compare well against the standard wall law profile. The turbulent flat plate flow simulated here had a Reynolds number of 2.0×10^6 per meter of plate length and a Mach number of 0.3. The grid dimensions were 100×100 and was decided upon after a grid independence study. Grid points were clustered to the wall in order to resolve the laminar sublayer. Characteristics based boundary conditions were specified for the inlet, outlet and free stream boundaries. A no-slip, adiabatic wall boundary condition was used at the surface of the flat plate. Comparison of the numerical results with analytical law of the wall profile is given in Fig. 1. The computed profile was taken at the end of the plate (x=1 meter). In the laminar sublayer, results collapsed onto wall law and around y^+ of 10 and above, the model began to show some differences but overall, it is good. The skin friction is plotted against the axial distance in Fig. 2. The model produces skin friction results slightly lower than the analytical curve (dotted). One reason is that the analytical model assumes that the flow is initially turbulent at the edge of plate but in the numerical results, the inlet flow was assumed to be laminar. Here, u^+, y^+, C_f are dimensionless velocity and dimensionless distance from the wall and friction coefficient where $u^+ = u/u^*$, $u^* = \sqrt{\tau_w/\rho}$, $y^+ = u^* y/\nu$, $C_f = 2\tau_w/\rho U^2$. Here, U, ν, τ_w are inlet velocity and kinematic viscosity and wall shear stress, respectively. Figure 3 compares the numerical $\tilde{\nu}$ with the normal solution near the wall, $\tilde{\nu} = u^* \kappa y$. They collapse onto each other near the wall and show the accuracy of our numerical scheme.

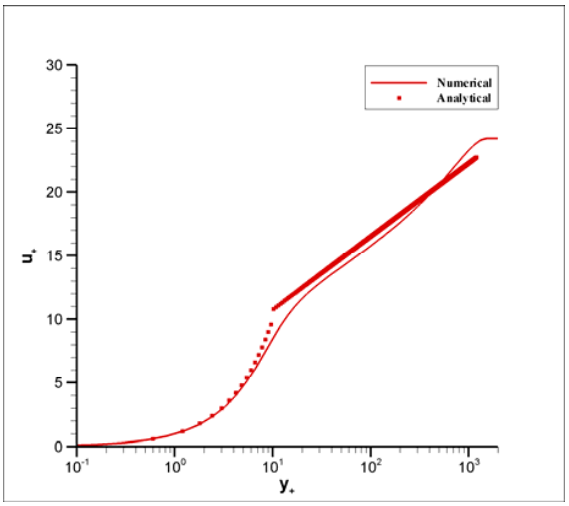

Fig.1 Comparison of numerical and analytical wall layer

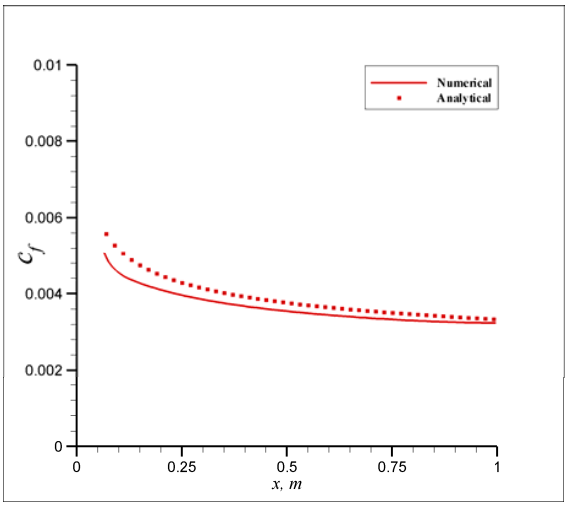

Fig.2 Comparison of numerical and analytical skin friction

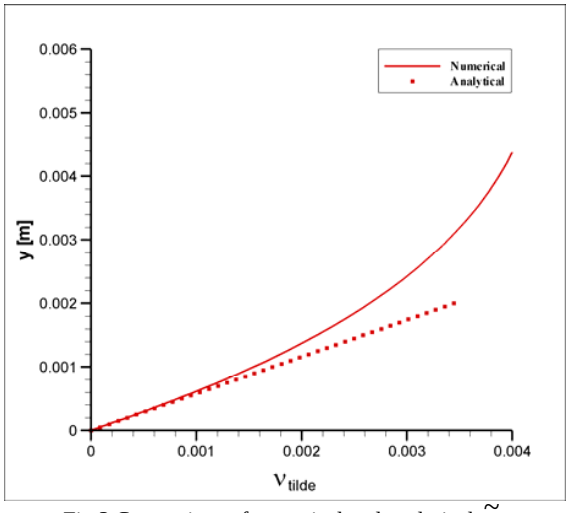

Fig.3 Comparison of numerical and analytical $\tilde{\nu}$

Next the experimental work of Driver and Seegmiller [16] is used for solution validation of the flow over a backward facing step. Their experiments were carried out in a 1.0 m long * 15.1 cm wide * 10.1 cm high rectangular inlet duct followed by a 1.27 cm backward facing step (h) in the floor. This configuration has a tunnel-width-to-step-height ratio of 12 to minimize the three-dimensional effects in the separated region, and a small expansion ratio to minimize the freestream pressure gradients. The freestream velocity is maintained at 44.2 m/s, which gives a Reynolds number of 37500 based on the step height. At the distance of four step-heights upstream of the step, the approaching wall boundary layer thickness was 1.9 cm. Under these conditions, fully developed turbulent layers are produced before passing over the step. The numerically determined reattachment point is at the distance x/h=6.0 downstream of the step, compared well to x/h=6.1 of the experimental results. Figure 4 compares the skin friction coefficient distribution along the wall obtained from the simulation to the experimental data.

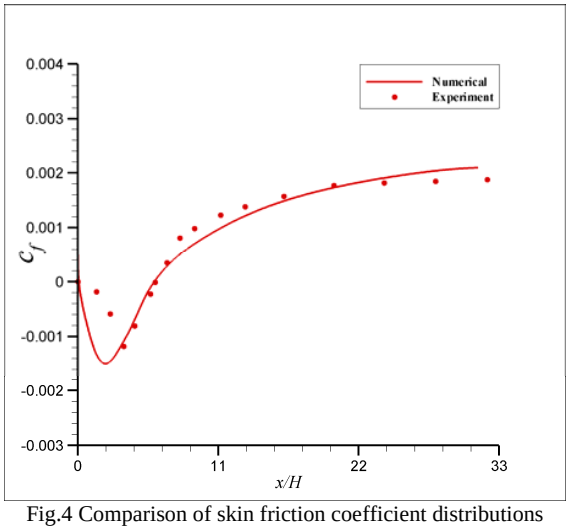

Fig.4 Comparison of skin friction coefficient distributions

The numerical simulation over predicted this quantity in the recirculating region, especially near the step face, but have shown good general agreement with the experimental data in the redeveloping region of the attaching turbulent boundary layer. More validation process may be found in reference 17. In this part, we present an analysis of the behaviour of a wall jet in turbulent regime by discussing the validity of S-A turbulence model used in our numerical study. First, the plane two-dimensional wall jet issuing to the quiescent field is considered for two different wall boundary conditions. Finally, the heat transfer in a wall jet at concurrent stream is analyzed numerically in an axisymmetric configuration. Figure 5 shows a jet discharged from a rectangular nozzle into stagnant surroundings, tangential to a flat plate. The width of the nozzle is very large compared to its height and thus we have a two dimensional wall jet. The Reynolds number, based on the jet exit velocity and the nozzle height, is 18000. The computational domain is 160b×40b where b is the nozzle height. Grid Clustering is used in both directions. At the nozzle exit, a uniform velocity profile is considered.

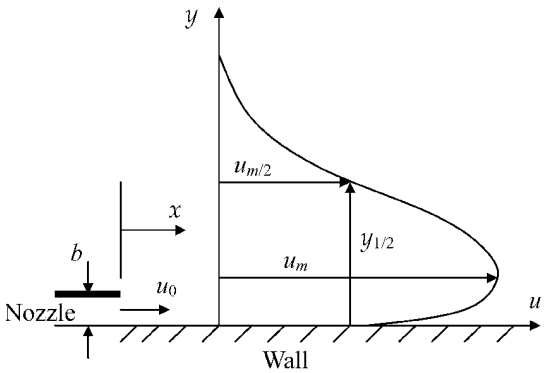

Fig.5 Flow configuration

Figure 6 compares predicted wall jet spreading rates along the plate to experimental measurements of Tailland [18] for an adiabatic wall case. It is noted that the S-A turbulence model adopted in this work has provided satisfactory results. Figure 7 shows the dimensionless profile of velocity u^+ with respect to y^+. This profile is presented for a section located in the similarity region of the wall jet and compared with experimental results of Nizou [19]. It is noticed that for low values of y^+ the prediction of u+ agrees well with the experiment. The wall law, $u^+= y^+$, is thus satisfied in the near wall region where the molecular viscosity becomes important. For y^+ higher than 10, there is a difference and the S-A model predicts lower u^+ than the experiment but the trends are similar. The wall friction coefficient C_f is defined here as the ratio of the wall shear stress to the dynamic pressure: $C_f=2\tau_w/\rho u_m^2$ where u_m is maximum local velocity. The Stream wise evolution of this coefficient is compared with experimental results of Tailland [18] in Fig. 8; the results are quite satisfactory.

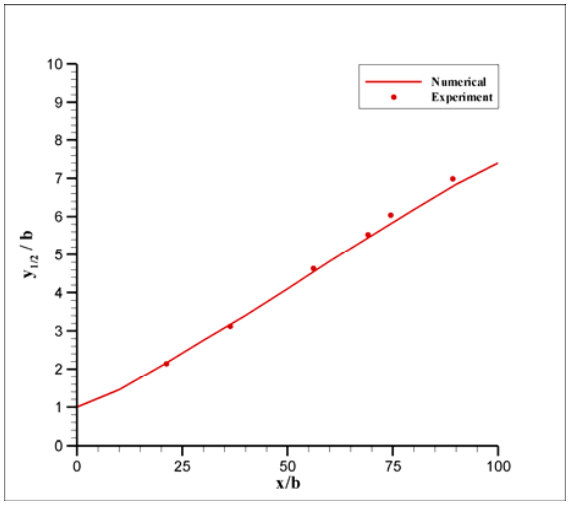

Fig.6 Stream wise development of the jet half width

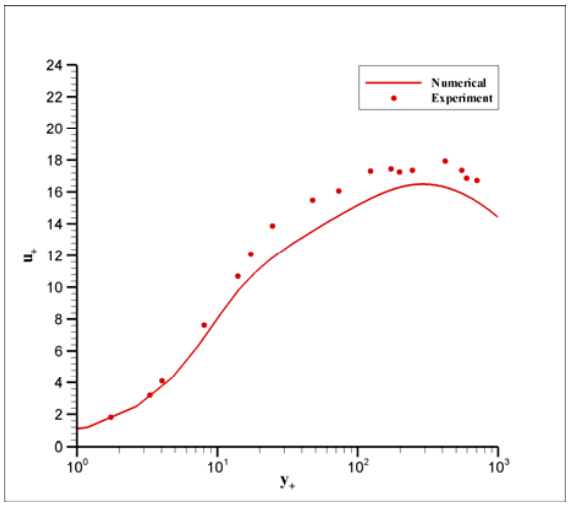

Fig.7 Dimensionless velocity profile

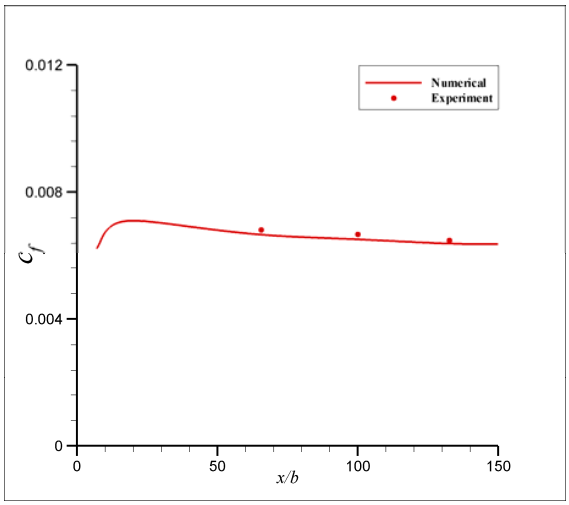

Fig.8 Stream wise development of the wall friction coefficient

To assess the ability of the turbulence model to predict the wall jet heat transfer coefficient, experiments conducted by Nizou [19] are used. In this case, the turbulent Prandtl number is 0.85 and 0.9 for comparison, and the molecular Prandtl number is 0.71. The Reynolds number is 14400. Figure 9 shows the profile of dimensionless temperature T^+ with respect to y^+. Here, $T^+=(T_w-T)/T_f$ and $T_f=\phi/\rho c_p u^*$ where T_w, ϕ, c_p are wall temperature, constant wall heat flux and specific heat of a gas at constant pressure, respectively. The temperature profile is given in a section located in the similarity region of the wall jet. It is noticed that for low values of y^+, numerical results correspond well to the relation $T^+ = Pr\, y^+$ which is valid in the zone close to the wall. Here, *Pr* is Prandtl number. The turbulence model results show satisfactory overall agreement with the experimental data. Turbulent Prandtl number has no sensible effect on the numerical result here.

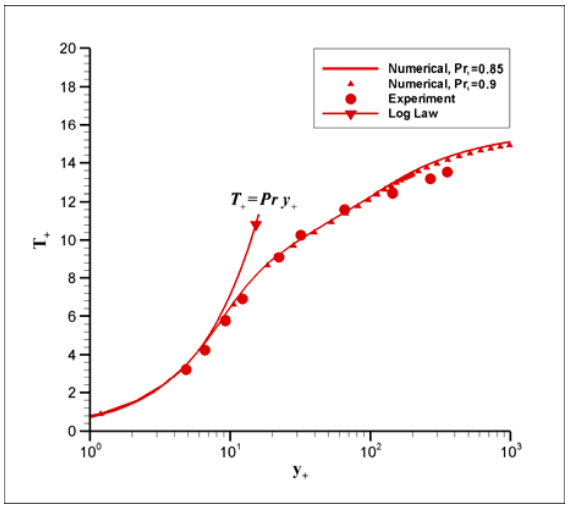

Fig.9 Dimensionless temperature profile

Finally, the heat transfer process is studied at an extending of a wall jet in a concurrent stream. The experiment of Lebedev et al. [20] is considered here. The tests were carried out in a cylindrical channel (80 mm diameter and 250 mm length). The wall jet was formed by blowing air through a tangential annular slot of height 2 mm. The schematic of problem geometry is shown in Fig. 10. This is an axisymmetric flow, so there are some additional parts in governing equations to simulate this problem and we added them for our study.

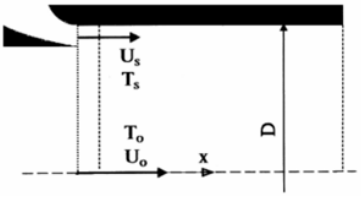

Fig.10 Flow configuration

Parameters of the main stream in the experiment were: U_o=15 m/s, Reynolds number 80000 based on U_o and D and T_o=300. Parameters of a wall jet were: U_s=36.3 m/s, Reynolds number 4000 based on U_s and slot width and T_s=363. The problem on the thermal mixing of a wall jet with a concurrent stream is usually considered for two types of boundary conditions: an adiabatic surface and a surface with a thermal flux. Using these results, the heat transfer coefficient $\alpha = q_w/(T_w - T_{wa})$ is determined where T_w, T_{wa} are the wall temperature in the non-adiabatic and adiabatic cases respectively. Subsequently, the simulations are carried out in two steps. First, the adiabatic case is solved and T_{wa} is determined. Then the channel is heated up in the regime q_w=constant and the wall temperature is calculated. Figure 11 represents the calculated heat transfer coefficient and compares it with the experimental result proposed by Lebedev. The model result has a good agreement with the experimental data, in a downstream of the flow field.

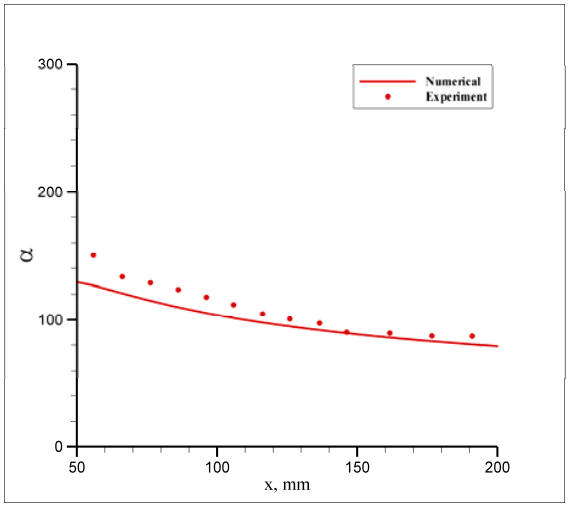

Fig.11 Heat transfer coefficient

IV. CONCLUSIONS

In this work, we have studied numerically the capability of the Spalart and Allmaras turbulence model for application in the wall jet flows. The wall jets considered here are both issuing to the stagnant surrounding and concurrent stream. A finite volume method with a non-uniform structured grid was carried out to solve the compressible flow using the AUSM$^+$ scheme.

Experimental data have been used to validations were in two-dimensional and axisymmetric cases. Both the fluid dynamic and thermal behaviour of turbulence model has been studied using the adiabatic and uniform heat flux boundary conditions. The results show good agreement with the experimental data for all mentioned features. Using this turbulence model in engineering applications may save the time cost of numerical predictions.

REFERENCES

[1] Nait Bouda, N., Schiestel, R., Amielh, M., Rey, C. and Benabid, T., "Experimental Approach and Numerical Prediction of a Turbulent Wall Jet over a Backward Facing Step," *International Journal of Heat and Fluid Flow*, Vol. 29, 2008, pp. 927-944.

[2] He, S., Xu, Z., and Jackson, J. D., "An Experimental Investigation of Buoyancy-Opposed Wall Jet Flow," *International Journal of Heat and Fluid Flow*, Vol. 23, 2002, pp. 487-496.

[3] Schober, M., and Fernholz, H. H., "Turbulence Control in Wall Jets," *European Journal of Mechanics B-Fluids*, Vol. 19, 2000, pp. 503-528.

[4] Adrian, H., and Law, W. K., "Measurements of Turbulent Mass Transport of a Circular Wall Jet," *International Journal of Heat and Mass Transfer*, Vol. 45, 2002, pp. 4899-4905.

[5] Kechiche, J., Mhiri, H., Palec, G., and Bournot, P., "Application of Low Reynolds Number *k*-e Models to the Study of Turbulent Wall Jets," *International Journal of Thermal Sciences*, Vol. 43, 2004, pp. 201-211.

[6] Craft, T. J., Gerasimov, A. V., Iacovides, H., Kidger, J. W., and Launder, B. E., "The Negatively Buoyant Turbulent Wall Jet: Performance of Alternative Opinion in RANS Modelling," *International Journal of Heat and Fluid Flow*, Vol. 25, 2004, pp. 809-823.

[7] Kechiche, J., Mhiri, H., Palec, G., and Bournot, P., "Numerical Study of the Inlet Conditions on a Turbulent Plane Two Dimensional Wall Jet," *Energy Conversion and Management*, Vol. 45, 2004, pp. 2931-2949.

[8] Cho, S. H., and Park, S. O., "Steady and Unsteady Computation of a Two-Dimensional Upwash Jet," *International Journal of Numerical Methods for Heat and Fluid Flow*, Vol. 8, No. 1, 1998.

[9] Aupoix, B., and Spalart, P. R., "Extensions of the Spalart-Allmaras Turbulence Model to Account for Wall Roughness," *International Journal of Heat and Fluid Flow*, Vol. 24, 2003, pp. 454-462.

[10] Nithiarasu, P., and Liu, C. B., "An Artificial Compressibility Based Characteristic Based Split Scheme for Steady and Unsteady Turbulent Incompressible Flows," *Computer Methods in Applied Mechanics and Engineering*, Vol. 195, 2006, pp. 2961-2982.

[11] Kral, L. D., "Recent Experience with Different Turbulence Models Applied to the Calculation of Flow over Aircraft Components," *Progress in Aerospace Sciences*, Vol. 34, 1998, pp. 481-541.

[12] Deck, S., Duveau, P., Espiney, P., and Guillen, P., "Development and Application of Spallart-Allmaras One-Equation Turbulence Model to Three-Dimensional Supersonic Complex Configurations," *Aerospace Science and Technology*, Vol. 6, 2002, pp. 171-183.

[13] Hirsch, C., Numerical Computation of Internal and External Flows, Wiley and Sons, New York, 1988.

[14] Spalart, P. R., and Allmaras, S. R., "A One Equation Turbulence Model for Aerodynamic Flows," *La Recherche Aerospatiale*, Vol.1, 1994, pp.5-21.

[15] Liou, M. S., "A Sequel to AUSM: AUSM$^+$," *Journal of Computational Physics*, Vol. 129, 1996, pp. 364-382.

[16] Driver, D. M., and Seegmiller, H. L., "Features of a Reattaching Turbulent Shear Layer in Divergent Channel Flow," *AIAA Journal*, Vol. 23, No. 2, 1985, pp. 163, 171.

[17] Tahsini, A. M., "Numerical Study of Solid Fuel Ignition Transient in Turbulent Flows," Doctoral Thesis, Sharif University of Technology, 2009.

[18] Tailland, A., "Contribution à L'étude d'un Jet Plan Dirigé Tangentiellement à une Paroi Plane," Doctoral Thesis, Université de Lyon, 1970.

[19] Nizou, P.Y., Tida, "Transferts de Chaleur et de Quantité de Movement dans les Jets Pariétaux Plans Turbulents," *International Journal of Heat and Mass Transfer*, Vol. 38, 1995, pp. 1187–1200.

[20] Lebedev, V. P., Lemanov, V. V., and Terekhov, V. I., "Heat Transfer in a Wall Jet at High Turbulence of Cocurrent Stream," *International Journal of Heat and Mass Transfer*, Vol. 42, 1999, pp. 599-612.